A Quantitative System for Studying Metastasis Using Transparent Zebrafish

Silja Heilmann[1], Kajan Ratnakumar[2], Erin M. Langdon[2], Emily R. Kansler[2], Isabella S. Kim[2], Nathaniel R. Campbell[3], Elizabeth B. Perry[2], Amy J. McMahon[4,5], Charles K. Kaufman[5,6,7,8], Ellen van Rooijen[5,6,7], William Lee[1], Christine A. Iacobuzio-Donahue[9], Richard O. Hynes[4,5], Leonard I. Zon[5,6,7,8], Joao B. Xavier[1], and Richard M. White[2,10]

Abstract

Metastasis is the defining feature of advanced malignancy, yet remains challenging to study in laboratory environments. Here, we describe a high-throughput zebrafish system for comprehensive, *in vivo* assessment of metastatic biology. First, we generated several stable cell lines from melanomas of transgenic mitfa-BRAF^{V600E};p53$^{-/-}$ fish. We then transplanted the melanoma cells into the transparent *casper* strain to enable highly quantitative measurement of the metastatic process at single-cell resolution. Using computational image analysis of the resulting metastases, we generated a metastasis score, μ, that can be applied to quantitative comparison of metastatic capacity between experimental conditions. Furthermore, image analysis also provided estimates of the frequency of metastasis-initiating cells ($\sim$1/120,000 cells). Finally, we determined that the degree of pigmentation is a key feature defining cells with metastatic capability. The small size and rapid generation of progeny combined with superior imaging tools make zebrafish ideal for unbiased high-throughput investigations of cell-intrinsic or microenvironmental modifiers of metastasis. The approaches described here are readily applicable to other tumor types and thus serve to complement studies also employing murine and human cell culture systems. *Cancer Res; 75(20); 4272–82. ©2015 AACR.*

Major Findings

- The zebrafish is an increasingly used model in cancer biology, owing to strengths in imaging and genetic tools afforded by the transparent *casper* strain of fish
- Transplantation of zebrafish BRAF^{V600E}-driven melanoma cell lines into *casper* allows for high-resolution imaging of each step of metastasis at single-cell resolution
- Quantitative imaging algorithms reveal strong tropism for skin, hematopoietic marrow, and eye, and a metastasis-initiating cell frequency of 1/120,000 cells
- Genetic manipulation of the zebrafish melanomas using CRISPR-mediated genome editing will allow for genome-wide *in vivo* screens to identify new metastatic modifiers
- These quantitative imaging tools can be rapidly applied to other cancer models increasingly available in the zebrafish

Introduction

Despite remarkable advances in elucidating the mechanisms of tumor initiation and growth, improvements in survival from metastatic cancer have remained elusive. In part, this is due to the difficulty of studying metastasis *in vivo* at large scale. Studies in murine systems have helped establish key steps in metastasis (1): local invasion at the primary site, intravasation into blood vessels at the primary site, circulation in the bloodstream, extravasation from blood vessels at distant sites, and the transition from micro to macrometastatic growth at distant sites after a period of dormancy. In individual patients, each of these steps is highly variable, likely in part due to the extreme heterogeneity across tumors. Moreover, it is increasingly recognized that the metastatic phenotype is intrinsically dependent upon interacting signals from the tumor and microenvironment (2, 3). Because of these factors, the study of metastasis requires an experimental system that allows for high-throughput manipulation of both tumor-cell and microenvironmental compartments.

In recent years, the zebrafish has emerged as an important model in cancer research (4), particularly in melanoma where

[1]Memorial Sloan Kettering Cancer Center, Computational Biology, New York, New York. [2]Memorial Sloan Kettering Cancer Center, Cancer Biology & Genetics, New York, New York. [3]Weill Cornell/Rockefeller/Sloan-Kettering Tri-Institutional MD-PhD Program, New York, New York. [4]Massachusetts Institute of Technology, David Koch Institute for Integrated Cancer Biology, Cambridge, Massachusetts. [5]Howard Hughes Medical Institute, Chevy Chase, Maryland. [6]Children's Hospital Boston, Boston, Massachusetts. [7]Harvard Medical School, Boston, Massachusetts. [8]Dana Farber Cancer Institute, Boston, Massachusetts. [9]Memorial Sloan Kettering Cancer Center, Pathology, New York, New York. [10]Weill Cornell Medical College, New York, New York.

Quick Guide to Equations and Assumptions

Estimating metastasis-initiating cell frequency

We assume that only a rare subpopulation of cells possesses the combination of traits, which enables them to leave the primary site, survive in circulation, and establish a metastasis large enough to be detected within the 14 days of the experiment—we dub these "metastasis-initiating cells" (MIC). We may then assume that when picking ZMEL1 cells at random, there is a fixed probability p of getting a cell with a stable metastasis-initiating phenotype. The probability of getting k MICs out of N randomly picked ZMEL1 cells must thus be given by the binomial distribution:

$$\Pr(k) = \frac{N!}{k!(N-k)!} p^k (1-p)^{N-k}.$$

The probability of getting no MICs out of N cells $(k = 0)$ is thus $\Pr(k = 0) = (1-p)^N$.

Poisson approximation to the binomial distribution

When N is large and p is small, the binomial distribution is well approximated by the Poisson distribution, with mean Np. This approximation is typically used if $N > 20$ and $P < 0.05$ or if $N > 100$ and $Np < 10$. Because we have $N > 10^4$ and most likely $P << 0.05$, we are able to use this approximation, so the probability of picking k MICs when randomly picking N cells is

$$\Pr(k) \approx (Np)^k \frac{\exp(-Np)}{k!}.$$

For $k = 0$, this becomes $\Pr(k = 0) = \exp(-Np) \Leftrightarrow log(\Pr(k = 0)) = -Np$, where N is the number of randomly picked cells from initial ZMEL1 population; k is the number of times an MIC (a cell with a metastasis-initiating phenotype) was picked out of the N random picks, and p is the probability of getting a cell with an MIC.

Metastasis score (μ score)

We wished to develop a score that captured metastatic burden across different sets of fish. We developed a weighted score, called the μ score, which incorporates multiple parameters captured from imaging. The measures m_i were chosen since they were the three top contributors to the first principal component (PC1) of the entire dataset. Further, the weights w_i were chosen to be similar to the weights of the three measures in PC1. Each measure was normalized by a fish-specific measure n_i of the same unit as m_i to make the terms of the sum dimensionless. These n_i were picked to be approximately equal to the upper limit, which the measures m_i can reach. The score can easily be modified to include additional measures m_4, m_5, ... if later needed. (Note that although it is numerically possible to reach a score of 100, it is not actually practically possible. Our highest scoring fish got a score of 50.)

$$\mu = 100 \sum_{i=1}^{3} w_i \frac{m_i}{n_i}$$

Measures characterizing metastatic growth: $m = [m_1, m_2, m_3]$.
Normalization factors for these measures: $n = [n_1, n_2, n_3]$.
Appropriate weights for each measure: $w = [w_1, w_2, w_3]$, where m_1 is the total summed area of metastases on day 14; n_1 is the area of fish body on day 14; w_1 is 1/2; m_2 is the AP distance on day 14; n_2 is the length of fish body on day 14; w_2 is 1/4; m_3 is the number of metastatic events on day 14; n_3 is L/2l (where L is the length of fish and l is the threshold for clustering metastases); and w_3 is 1/4.

transgenic expression of the human BRAF[V600E] gene leads to a fully penetrant disease that is similar to the human disease (5–7). Building upon these transgenic models, we have developed a high-throughput system for studying metastasis that is composed of two separate toolsets: (i) zebrafish melanoma cell lines with defined genetic and phenotypic characteristics as a source of donor tumor cells, and (ii) a highly quantitative metastasis transplantation assay using the transparent *casper* strain (8, 9) of zebrafish as a recipient host. The *casper* strain maintains relative transparency throughout life and is particularly suited to quantitative assessment of spatio-temporal dynamics of metastasis, allowing us to build statistical pictures of metastatic patterns with unprecedented detail. Dramatic advances in zebrafish genome manipulation using CRISPR (10, 11) technologies allow us to

easily modify both our zebrafish melanoma cell lines and the *casper* recipient. Taken together, our system provides the first high-throughput method to probe metastatic biology *in vivo*, which will be broadly applicable to researchers across the cancer spectrum.

Materials and Methods

MiniCoopR transgenic melanoma fish and isolation of the ZMEL1 cell line

Transgenic melanoma zebrafish using the MiniCoopR system were created as previously described (7). Briefly, a plasmid was created in which the zebrafish mitfa promoter drives a zebrafish MITF minigene devoid of introns. On the same plasmid was a second cassette in which the mitfa promoter drives EGFP.

Flanking both of these genes are Tol2 transposon arms. This plasmid was injected into fish with the following genotype: mitfa-BRAF^{V600E};p53$^{-/-}$;mitfa$^{-/-}$. This strain of fish is devoid of all melanocytes (due to the mitfa$^{-/-}$ mutation), but upon mosaic rescue with the mitfa-MITF minigene will develop "patches" of rescued melanocytes, some of which will go on to develop melanoma during adulthood. Because the rescued melanocytes all contain the MiniCoopR plasmid, they will necessarily also express mitfa-EGFP, resulting in melanomas that are entirely EGFP positive. For the isolation of the cell lines, tumors were cleanly dissected with a scalpel from melanoma-bearing Mini-CoopR fish and transferred to a small petri dish containing 2 mL dissection medium (50% Ham's F12/50% DMEM, 10× Pen/Strep, 0.075 mg/mL Liberase). They were then manually disaggregated for 30 minutes at room temperature. An inactivating solution (50% Ham's F12/50% DMEM, 10× Pen/Strep, 15% heat-inactivated FCS) was then added, and the suspension was filtered 2 to 3× in a 40-μm filter. This was then centrifuged for 5 minutes at 500 rcf, and resuspended in 500 μL of complete zebrafish media (Supplementary Methods for further details). This 500 μL was then plated in a single well of a 48-well plate that has been previously coated with fibronectin.

Proliferation assays/drug treatments

Cells were plated at a density of 25,000 to 50,000 cells per well in a 96-well plate in 100 μL of DMEM/10. The cells were allowed to adhere for 24 hours, and then media changed to fresh media containing either DMSO or drugs at the indicated doses. The final concentration of all wells contained equivalent amounts of DMSO solvent (1%). The media were refreshed every 2 days, and at day 5, Alamar blue was added and fluorescence read using a 96-well plate reader. All values were normalized to the DMSO control well, and done in at least triplicate for each day of experiments.

RNA-seq of ZMEL1

Reads from each RNA-Seq run were mapped to the zebrafish reference genome version danRer7 from the UCSC Genome Browser (12) using GSNAP and quantified on the gene level using HTSeq and Ensembl version 75. Differential expression analysis was performed using DESeq2. The 40-bp single-end and 100-bp paired-end runs of ZMEL1 were used as separate replicates. Runs ERR004009, ERR004010, ERR004011, ERR004012, and ERR015568 from ENA study ERP000016 (13) were used as normal samples.

Reagents

The plasmids used for the MiniCoopr transgenics were obtained as a gift from Yariv Houvras (Weill-Cornell Medical College). The Cas9 plasmid was obtained from Addgene (#42251). All cell culture media (as outlined in Supplementary Methods) were obtained from Life Technologies. PLX4032 was a gift from Plexxikon, and CI1040 was obtained from Selleckchem (catalogue number S1020).

Animal husbandry

All zebrafish were housed in a temperature (28.5°C) and light-controlled (14 hours on, 10 hours off) room. Fish were initially housed at a density of 5 to 10 fish per liter, and fed 3 times per day using brine shrimp and pelleted zebrafish food. After transplan-

tation, the fish were housed in individual chambers for serial imaging. All anesthesia was done using Tricaine (Western Chemical Incorporated) with a stock of 4 g/L (protected for light) and diluted until the fish was immobilized. All procedures adhered to IACUC protocol #12-05-008 through Memorial Sloan Kettering Cancer Center.

Imaging and image analysis

Equipment. All fish were anesthetized with Tricaine and placed onto a petri dish. The fish were imaged from above using a Zeiss Axio Zoom V16 Fluorescence Stereo Zoom Microscope with a 0.6× or 1.6× lens. Each fish was successively imaged using brightfield, GFP, and Rhodamine filter sets on both sides. The exposure times for each group were determined at day 1 and kept fixed throughout the entire experiment. If the fish was larger than a single field, then multiple images for each fish was taken using a motorized stage and stitched together using the Zeiss Zen software. Raw image files (CZI) for each fish were then exported using Zen as high-resolution TIFFs that could then be used for downstream image analysis in MATLAB. The MATLAB code used for all analyses is available online (14).

Image registration/image transformations. Each adult fish in the study ($n = 106$) was imaged at three different time points (days 1, 7, and 14 after implant). At each time point, brightfield, GFP, and RFP channel images were taken of both the right and the left sides of the fish. After the images had been transformed and registered using landmarks, they could be superimposed allowing for comparison of (i) left and right side images of each fish, (ii) same fish imaged at a different time points, and (iii) images of different fish with each other. The transformations were done using a custom fully automated image registration pipeline; see further details in Supplementary Methods and Supplementary Figs. S16–S20. The MATLAB code for all image analysis is available online (14).

Principal component analysis

We were interested in extracting features from the segmented images, which in different ways characterized/quantified the growth of the tumor and the metastasis formation over time. We initially extracted 15 features (Supplementary Table S3), and from this initial pool found the following 5 to be most informative:

1. Solidity (ratio of total area of GFP region to area of smallest convex polygon, which will encapsulate the GFP region. This measure will give a value close to one, for example, a solid sphere or triangle and a low value for a very fragmented or fractal like region).
2. Area of primary tumor.
3. Total area of all metastasis.
4. Number of metastatic events (number of times a new metastasis occurs).
5. Anterior–posterior distance of tumor/metastasis [the length between the two pixels that are the furthest apart (regardless of whether they belong to primary or metastatic regions) measured along the anterior–posterior axis of the fish].

These five features were extracted from the images taken at the three different time points, meaning that each fish became

represented by a point in a 15-dimensional feature space. In order to determine which of these features were primarily responsible for the variance across the group and also to determine which features were correlated/anticorrelated/uncorrelated, we did principal component analysis (PCA) on the data. Because PCA is sensitive to the scaling of the variables, we normalized all measures by the variance in the group of that measure on the day 14 time point, before performing the analysis. For example:

1. Solidity_D1_normalized = Solidity_D1/var(Solidity_D14).
2. AreaPrimary_D7_normalized = AreaPrimary_D7/var (AreaPrimary_D14).
3. TotalMetsArea_D7_normalized = TotalMetsArea_D7/var (AreaPrimary_D14).
4. AP_distance_D14_normalized = AP_distance_D14/var (AP_distance_D14).

With this normalization, the PCA will reveal which features contributed most to the overall variance in the dataset while still keeping different measures that are sharing the same basic unit on the same scale (like AreaPrimary_D7 and TotalMetsArea_D14, which both have unit length^2).

Metastasis-initiating cell frequency

One hypothesis about metastasis formations is that only a rare subpopulation of cells possesses the combination of traits, which enables them to leave the primary site, survive in circulation, and establish a metastasis large enough to be detected within the 14 days of the experiment. If this hypothesis holds, we may assume that when picking ZMEL1 cells at random there is a fixed probability, p, of getting a cell with a stable metastasis-initiating phenotype. The probability of getting k metastasis-initiating cell (MIC) out of N randomly picked cell must thus be given by the binomial distribution

$$\Pr(k) = \frac{N!}{k!(N-k)!}p^k(1-p)^{N-k}.$$

The probability of getting no MICs ($k = 0$) is thus

$$\Pr(k = 0) = (1-p)^N. \quad (1)$$

Based on the original implant size group and the area and fluorescence intensity in images taken on day 1, we estimated the number of cells that were successfully implanted in fish number i at day 0, N_i, for each fish (see Supplementary Methods for the details of how we did this estimate). By day 14, each fish either has at least one metastasis or none, i.e., $\Pr_i(k = 0)$ of fish i is either 1 or 0. We fit the points $[N_i, \Pr_i(k = 0)]$, using nonlinear regression (to equation 1) and was thus able to estimate the parameter p, which is the frequency of MICs in the ZMEL1 population. We found this frequency to be $p = 8.4 \times 10^{-6}$ (i.e., 1 of ~120,000 cells is capable of forming a macro-metastasis within the timespan of 14 days).

Poisson approximation. When N is large and p is small, the binomial distribution is well approximated by the Poisson distribution, with mean Np. This approximation is typically used if $N > 20$ and $P < 0.05$, or if $N > 100$ and $Np < 10$. Because we have $N > 10^4$ and most likely $P < <0.05$, we are able to use this approxi-

mation, so the probability of picking k MICs when randomly picking N cells is

$$\Pr(k) \approx (Np)^k \frac{\exp(-Np)}{k!}.$$

We expect the probability of having no metastasis to depend on N in the following manner:

$$\Pr(k = 0) = \exp(-Np) \Leftrightarrow$$
$$\log(\Pr(k = 0)) = -Np. \quad (2)$$

We see from equation 2 that we can expect that log ($\Pr(k = 0)$) for the three implant size groups small, medium, and large, plotted versus N to follow a straight line going through (0,1) and p, the frequency of MICs, will be the slope of this straight line. As seen in Fig. 5, the points for three size groups small, medium, and large do not show a linear dependency, but rather suggest a convex dependency. Nonetheless, the precision of the estimate is not sufficient to refute the existence of a subpopulation of MICs.

Results

Generation of zebrafish melanoma cell lines

Previous work (5–7) has established a transgenic zebrafish model of human melanoma, in which expression of human BRAF^{V600E}, under the melanocyte-specific mitfa promoter, leads to rapid formation of pigmentation abnormalities and nevi. When crossed with p53$^{-/-}$ fish, 100% of the resultant animals (mitfa-BRAF^{V600E};p53$^{-/-}$) develop melanomas in highly stereotyped locations, including the head, dorsal skin, and caudal fin. Although these animals have previously been used to identify genes and chemicals (6, 7), which affect melanoma initiation, the metastatic characteristics of these tumors have not been defined. To assess this, we performed a series of transplant studies of primary tumors into the transparent *casper* strain of zebrafish. The recipient fish developed highly variable degrees of metastatic dissemination (Supplementary Fig. S1). This metastatic heterogeneity is likely due to the tremendous genetic heterogeneity that we have previously found to be present in the transgenic zebrafish melanomas (15). This observation prompted us to develop stable cell lines from the zebrafish tumors, which would lead to more reproducible metastatic behavior upon transplantation, as has been shown for human tumors (16, 17). Adopting methods commonly used for isolation of human melanoma lines, we developed fluorescently labeled stable zebrafish melanoma cell lines. We generated a large number of primary transgenic tumors using the MiniCoopR transposon system, which allows mosaic expression of the BRAF^{V600E} in a p53$^{-/-}$ background, and generates transgenic animals with melanoma within 2 to 3 months (7). The MiniCoopR transposon also carries a mitfa-GFP cassette; because mitfa is only expressed by melanocyte derivatives, the presence of GFP confirms its lineage identity as a *bona fide* melanoma line. We isolated a series of these transgenic mitfa-BRAF^{V600E};p53$^{-/-}$;mitfa-GFP tumors (an example is shown in Fig. 1A), disaggregated them into single-cell suspension, and plated them on fibronectin-coated plates in a media formulation similar to that used to isolate human melanoma cell lines from patients (18, 19). We then allowed these cells to propagate over
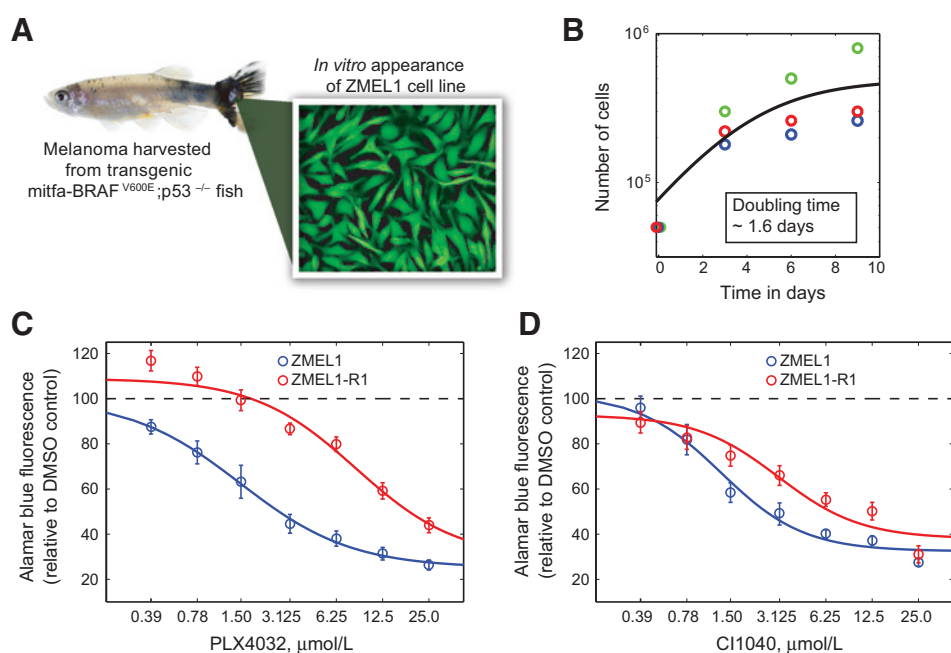
Figure 1.
Derivation and characterization of the ZMEL1 zebrafish melanoma cell line. A, representative melanoma-bearing fish (left) from the MiniCoopr background, which mosaically expresses BRAF^{V600E} in a mitfa-GFP; p53$^{-/-}$ background, and yielded the stable cell line ZMEL1, which is uniformly GFP positive. B, growth curves of the ZMEL1 line demonstrate a population-doubling time of 1.6 days. Individual colors represent replicate experiments. C and D, the response of the ZMEL1 and ZMEL-R1 lines to either the BRAF^{V600E} inhibitor PLX4032 (C) or the MEK inhibitor CI1040 (D). The resistant line demonstrates an 8-fold increase in the EC$_{50}$ to the BRAF inhibitor, but only a 2-fold increase in the EC$_{50}$ to the MEK inhibitor.

time in order to select tumors that ultimately gave rise to stable cell lines.

Overall, we successfully established 31 stable cell lines, out of 43 attempts, for a success rate of 72% (Supplementary Table S1). All but one of these could be transitioned off of fibronectin onto plastic plates. For the purposes of demonstration, we focused on one particular line, which we refer to as ZMEL1 (Zebrafish Melanoma line 1, as shown in Fig. 1A) because of the following key characteristics: after the 10th passage, we were able to transition the line off the more complex isolation medium to standard DMEM with 10% FCS, and could eliminate the need for fibronectin coating of the plates. By FACS sorting, ZMEL1 showed greater than 99.5% GFP-positive cells, indicating essentially no contaminating stromal cell elements. The population doubling time (Fig. 1B) of approximately 1.6 days makes it amenable to generating large numbers of cells rapidly. We maintain the ZMEL1 line at 28.5C/5% CO$_2$ in a standard tissue culture incubator. The ZMEL1 line can be transfected with expression vectors of interest using nucleofection technology. For example, nucleofection of an ubiquitin-EGFP-2A-tdTomato plasmid, followed by repeated FACS sorting, led to establishment of a stable cell ZMEL1 line expressing both eGFP and tdTomato (Supplementary Fig. S2). We repeated this for additional genes, including CFP and YFP, all using the 2A system, and were able to generate either transient or stable cell lines for all constructs (data not shown). We also asked whether we could knockout gene function using CRISPR technology. We nucleofected a CMV-Cas9 plasmid along with a plasmid containing a guide RNA against eGFP (driven by the zebrafish U6 promoter). After blasticidin selection, we were able to obtain a stable cell line in which approximately 99% of the cells no longer expressed eGFP (Supplementary Fig. S3). We confirmed mutagenic efficiency of the eGFP gene using both FACS and the Surveyor nuclease assay (Supplementary Fig. S4). Taken together, these data indicate that the ZMEL1 line can be genetically modified and will readily allow both overexpression (cDNA) and knockout (CRISPR) screens.

Cross-species transcriptomic analysis

To determine the similarity between the ZMEL1 line and human melanoma, we compared the transcriptomic profile of ZMEL1 to human cancer cell lines using GSEA (20). We performed RNA-seq analysis of the ZMEL1 line (Supplementary Table S2) and identified the 250 most up- or downregulated genes in ZMEL1 (compared with pooled normal reference RNA). We then compared that signature via GSEA with the human NCI60 gene signatures (Supplementary Figs. S5 and S6; and Supplementary Table S2; ref. 21). This revealed a striking enrichment of the ZMEL1 signature in human melanoma cell lines (i.e., MALME-3M and SK-Mel28) compared with all other tumors (normalized enrichment score = 1.702, FDR = 0.0012). Among the most upregulated genes in both human and zebrafish melanoma are factors known to be expressed in neural crest-derived melanocytes, including *sox10, ednrb,* and *mitfa* itself. These are genes also known to play pathogenic roles in human melanoma, either through overexpression or amplification (22–28). We also used GSEA to compare the ZMEL1 signature to previously established gene signatures from transgenic mitf-BRAF^{V600E};p53$^{-/-}$ primary tumors (6), and again found a strong similarity to the original tumors (Supplementary Figs. S7 and S8; Supplementary Table S2). Finally, we analyzed the ZMEL1 RNA-seq signature using Ingenuity Pathway Analysis (Supplementary Figs. S9 and S10). This revealed a strong enrichment for pigment cell signaling, as well as a dependence upon MYC signaling, as expected for a tumor driven by BRAF^{V600E}. Taken together, the transcriptomic data demonstrate that the ZMEL1 line strongly resembles well-characterized transgenic zebrafish melanomas as well as human melanoma cell lines.

ZMEL1 sensitivity to MAP kinase inhibition

We next confirmed functional dependency on BRAF-MAP kinase signaling using pharmacologic inhibition. We treated the ZMEL1 line with either the BRAF^{V600E} inhibitor PLX4032 (29) or the MEK inhibitor CI1040 (30) and measured proliferation at 5

days using the Alamar blue assay (Fig. 1C and D). Both of these drugs caused a dose-dependent inhibition of ZMEL1 proliferation, with an EC_{50} of 1.12 μmol/L and 1.30 μmol/L, respectively. To further confirm the functional similarity to human melanoma cell lines, we determined whether ZMEL1 could become BRAF inhibitor resistant *in vitro*, as has been widely reported for human melanoma lines (31, 32). We treated the ZMEL1 line with 1 μmol/L PLX4032 over a period of several months, which led to a rapid loss of most viable cells by 1 week, as expected, but a small population of persister cells remained. By 3 to 4 months, these cells had become resistant to this concentration of PLX4032 and reconstituted the culture. We then retested sensitivity to both PLX4032 and CI1040 (Fig. 1C and D). The EC_{50} for PLX4032 increased 7.6-fold (from 1.13 μmol/L to 8.56 μmol/L). The cells remained moderately sensitive to MEK inhibition, with only a 2.3-fold increase in the EC_{50} for CI1040 (from 1.30 μmol/L to 3.06 μmol/L). This derivative line, which we refer to as ZMEL1-R1 (ZMEL1-resistant line 1), demonstrates that zebrafish melanoma cell lines react to MAP kinase inhibition in a manner analogous to their human counterparts. The genetic mechanism resulting in such resistance remains to be elucidated and will be the subject of future studies.

Metastatic behavior of the ZMEL1 line

We next determined the metastatic capacity of the ZMEL1 line. We took advantage of the previously described *casper* strain of zebrafish, which maintains relative transparency throughout its entire life cycle and allows highly sensitive detection of fluorescently labeled cells anywhere in the animal at single-cell resolution (8, 9). We transplanted ZMEL1 cells into either adult or embryonic *casper* recipients using a quartz glass microcapillary needle attached to a microinjection apparatus (Fig. 2). For the adult fish, we transplanted 500,000 ZMEL1 cells into the subcu-

taneous tissue of the ventral flank of a recipient that had been previously irradiated with a total of 30 Gy (15 Gy × 15 Gy split dose over 2 days). We found that irradiation of the adult recipient was required due to MHC mismatch between the ZMEL1 line and *casper* recipients. For the embryos, we transplanted 150 ZMEL1 cells directly into the vasculature (via the Duct of Cuvier). The embryos recipients did not require any preconditioning radiation since they do not yet have a mature adaptive immune system. MHC mismatch, the major cause of implant rejection, depends upon the adaptive response, which does not develop in the zebrafish until approximately 14 days of life. The adult assay allows for full assessment of metastasis from an orthotopic site but requires immunosuppression; the embryonic assay allows for direct intravascular injection of tumor cells and requires no immunosuppression.

Representative fish are shown in Fig. 2. In the adult recipients (Fig. 2, left), at 1 day after transplant, a brightly GFP⁺ mass can be seen at the site of injection with little or no distant metastases. By 1 week, and then 2 weeks after transplant, the size of the mass at the injection spot continued to grow, as expected, along with the appearance of multiple new anterior masses. These masses are clearly distinct from the site of implantation and represent distant metastases. In the embryo recipients (Fig. 2, right), at day 1 after transplant, the cells circulate primarily within the ventral vasculature (Supplementary Video S1) and have begun to extravasate into the caudal hematopoietic tissue, the first site of definitive hematopoiesis in the fish. By 1 week and then 2 weeks, all of the cells have extravasated, and the fish develops GFP⁺ tumors in the eye, kidney, muscle, and head. This leads to the death of the animals by 30 to 60 days after transplant. One major advantage of these embryo transplants is that single-cell behavior is easily observed after transplantation. Taken together, these data indicate that the ZMEL1 line is capable of performing all of the canonical steps of metastasis.
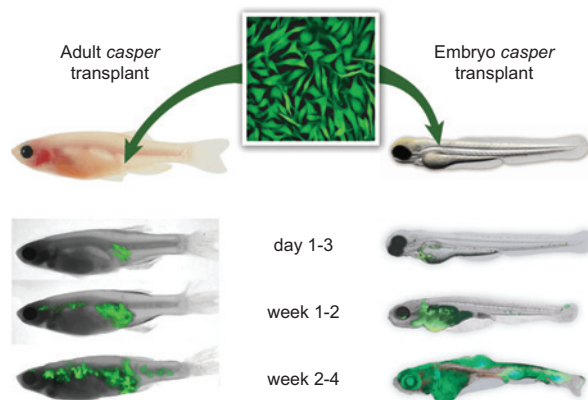
Patterns of metastatic spread

In order for this assay to be useful as a screening tool, we needed to develop automated quantitative imaging of metastasis. We reasoned that the degree of metastatic dissemination would be dependent upon the number of cells transplanted into the *casper* recipient, and should vary with both site of implantation and time after transplant. We therefore performed a series of limiting dilution transplantation studies in which we varied the cell number (1×10^5, 5×10^5, 1×10^6) and the transplant site (dorsal vs. ventral skin). We then imaged each fish at 1 day after transplant, 7 days after transplant, and 14 days after transplant using both brightfield and GFP, on both the left and right sides of the fish. We developed a custom-designed computer image analysis algorithm in MATLAB to align each image such that it could be precisely overlaid with all of the others. Landmarks such as the center of mass of the eye, the anterior end of the spine, and dorsal and ventral boundary points were used to guide image alignment transformations, and the images from the GFP channel were subsequently analyzed using a custom image segmentation algorithm to detect location of primary tumor and metastasis. Because transplantation itself has some degree of mechanical variability, we imaged each fish on day 1 and used information from these images along with the information of the original cell dose to better estimate the number of cells that each recipient actually received. This is a major advantage of the fish compared with mouse studies, where accounting for such mechanical variability
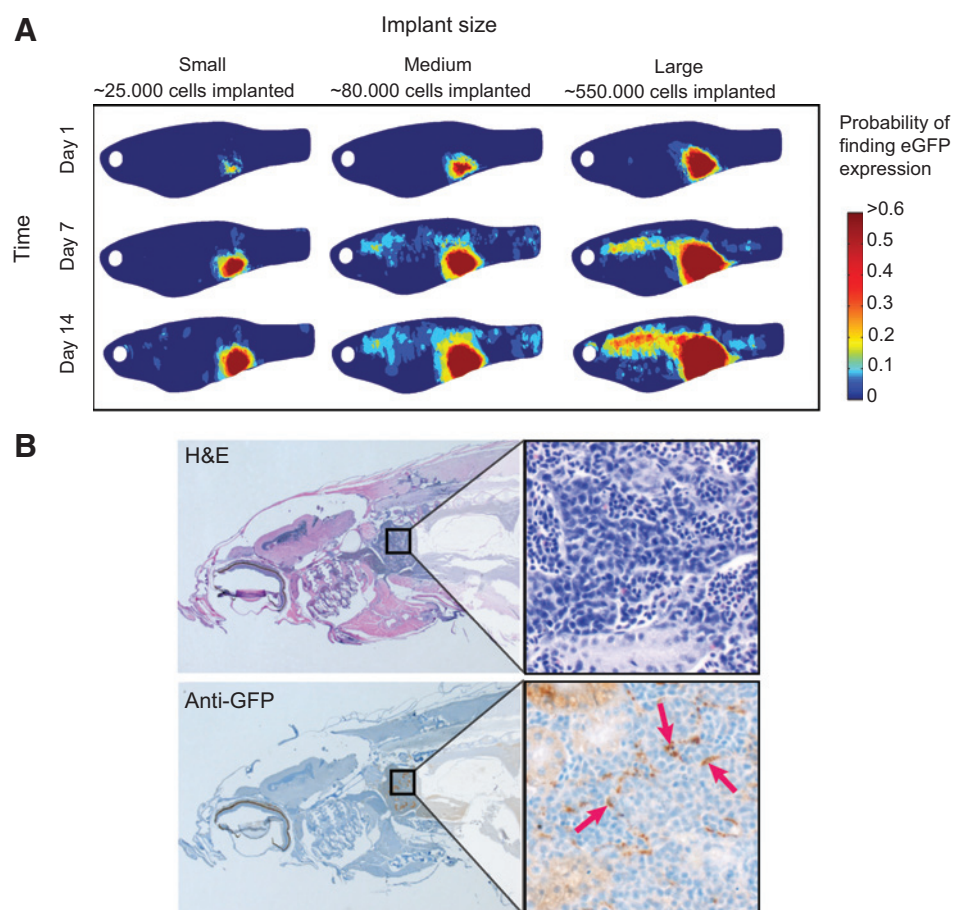

Figure 2.
Evaluating metastasis of the ZMEL1 line using transplantation into the transparent casper recipient line. ZMEL1-GFP cells can be transplanted either subcutaneously into the flank of an irradiated casper recipient (left) or directly into the vasculature of an unirradiated casper embryo at 2 days after fertilization (right). The fish were then imaged over a period of approximately 1 month using GFP and brightfield imaging. Representative fish for both assays are shown. For the adults, approximately 500,000 cells were transplanted, and for the first 1 to 3 days after transplant, the cells remained localized, but by weeks 1 to 4, they widely disseminated anteriorly and posteriorly from the initial implant site. A similar pattern is seen in the embryo transplants, but because the cells were injected directly into the circulation, extravasation and formation of disseminated masses occurred more rapidly.

Figure 3.
Analyzing the pattern of metastatic spread after ZMEL transplantation. A, composite heatmap images of a group of fish ($n = 53$) transplanted with small ($\sim$25,000 cells, $n = 19$), medium ($\sim$50,000 cells, $n = 20$), or large cell numbers ($\sim$500,000 cells, $n = 14$) at day 1, and then imaged at days 7 and 14. The heatmap corresponds to the probability of finding GFP$^+$ ZMEL1 cells at the given location. This demonstrates that the likelihood of metastasis varies with the number of cells transplanted. The GFP-positive masses seen anteriorly at day 14 are suggestive of localization within the kidney marrow, the site of hematopoiesis in the zebrafish. This localization was confirmed using histologic sectioning of a representative fish (B), stained with either H&E (B, top) or an anti-GFP antibody (B, bottom). Brown staining (denoted by red arrows) indicates the presence of ZMEL1-GFP cells in the kidney marrow compartment.

is not possible. After this determination, we appropriately regrouped the fish into small ($25,700 \pm 24,560$ cells), medium ($80,544 \pm 52,358$ cells), and large ($552,720 \pm 272,030$ cells) implant sizes (see Supplementary Methods for details on estimation procedure). We used data collected from 106 fish to create composite heatmap images of metastatic progression from cells transplanted either ventrally (Fig. 3A) or dorsally (Supplementary Fig. S11). This revealed a strong correlation between size of the initial implant and the likelihood of metastasis. Small implants on day 1 generally produced fish with few metastases at day 14, whereas those with large masses on day 1 led to a large increase in the metastatic burden, particularly in the anterior region just behind the gill structure, as well as scattered other metastases to the posterior tail musculature and eye. This dissemination pattern was not due to the implant site, as we saw similar patterns whether the cells were transplanted dorsally or ventrally. Overall, 83% (25/30) of fish in the large implant group had metastases at day 14, compared with 44% (18/41) in the small implant group. We noted on the heatmaps that some of the anterior metastases anatomically corresponded to the area of the kidney marrow, the region of hematopoiesis in the zebrafish (33). To confirm this, we performed histologic analysis on a series of fish at 2 weeks after transplant (Supplementary Fig. S12). This showed that fish with higher cell doses had clear metastases in the kidney marrow [by both hematoxylin/eosin (H&E) and anti-GFP imaging], an example of which is shown in Fig. 3B. To determine if this tropism was an artifact of the transplant technique, we performed RNA *in situ*

staining in three of the original mitfa-BRAF^{V600E};p53$^{-/-}$ transgenic fish, from which ZMEL1 was derived. We stained for expression of the neural crest marker crestin, a retroelement normally only expressed in embryonic neural crest cells (34), which becomes aberrantly expressed exclusively in adult melanomas due to its neural crest origins (6). One of the three fish had evidence of metastases to the kidney (Supplementary Fig. S13), indicating that the transplanted cells have a tropism for the kidney marrow similar to melanoma developed spontaneously in the stable transgenic mitfa-BRAF;p53$^{-/-}$ fish line. These data are consistent with other reports indicating a tropism of human melanoma cells for the bone marrow in mammalian systems (35–37).

Development of a metastasis score (μ score)

Although the heatmap views are useful for determining overall patterns of spread, they do not allow for a simple quantification of overall metastatic burden. We wished to develop a straightforward "metastasis score," μ, which would be of general use to the community and to determine how this score differed between the three implant size groups. Initially, we extracted 15 parameters from the images taken at three separate time points (e.g., area of primary tumor, area and number of metastasis, length of fish body, see Supplementary Table S3 for the complete list of features) and then used PCA to determine which parameters best explained the variance in the data. The PCA (Fig. 4A) demonstrated that just three of these parameters at day 14 accounted for a substantial amount of the variance in the data, which was related
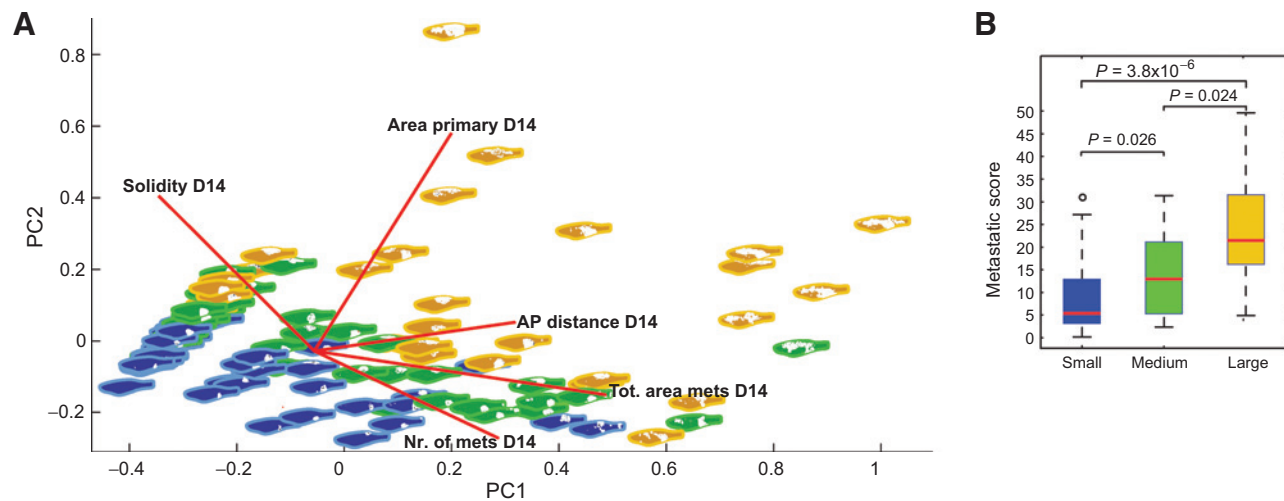
Figure 4.
Quantification of metastatic burden in the zebrafish. A, PCA plot of the major variables measured in each fish at days 1, 7, and 14 [area of the primary, total area of metastases, total number of metastases, solidity of primary tumor, and anteroposterior (AP) distance from primary to metastases]. Blue fish correspond to "small" implant size at day 1, green to "medium" implant, and yellow to "large" implant. B, the μ score as a measure of metastatic burden. Using the top three contributors to principal component 1 described in A and Supplementary Fig. S10, we calculated a dimensionless μ score (metastasis score) for fish with small, medium, or large implant tumors at day 1. See Quick Guide to Equations and Assumptions and Supplementary Fig. S14 for the definition of the μ score. This demonstrates that the size of the implant at day 1 strongly predicts metastasis at day 14, with a significantly greater μ score in medium or large groups compared with the small group (P values as indicated from the two-sample KS test).

to formation of metastasis: (i) total number of metastases, (ii) total area of metastases, and (iii) anteroposterior distance spanned by both primary and metastases. We combined the three parameters into a simple dimensionless μ score, which can easily be applied in other studies (Supplementary Fig. S14). We calculated the median μ score for each of the three implant size groups (Fig. 4B): At day 14 for the group with small implants, it was 5.35, whereas for the medium group, it was 12.94, and for the large group, it was 21.42. The difference between the μ score distributions was significant for small versus medium [$P = 0.026$, two-sample Kolmogorov–Smirnov (KS) test], medium versus large ($P = 0.024$, two-sample KS test), and small versus large (3.75×10^{-6}, two-sample KS test). The μ score can be applied to future

experimental interventions (i.e., overexpressing or knocking down specific genes) allowing for a rapid and quantifiable assessment of metastatic efficiency.

Quantification of metastasis with MIC frequency

We next wished to estimate the frequency of MICs, analogous to the tumor-initiating cell calculations frequently employed for quantifying cancer stem cells. Using standard limiting dilution analysis (38, 39), we determined the number of animals with or without metastases at day 14 using either the intended cell numbers (Supplementary Fig. S15) or after regrouping into the estimated small/medium/large groups (Fig. 5). Since we found that regrouping more accurately reflects the actual number of cells

Figure 5.
An estimation of MIC frequency. The estimated number of cells present at day 1 (x-axis) is correlated with the proportion of fish that do or do not have metastasis at day 14 (y-axis). Limiting dilution analysis allows for an estimation of MIC frequency of 1/119,311 cells for the ZMEL1 line.
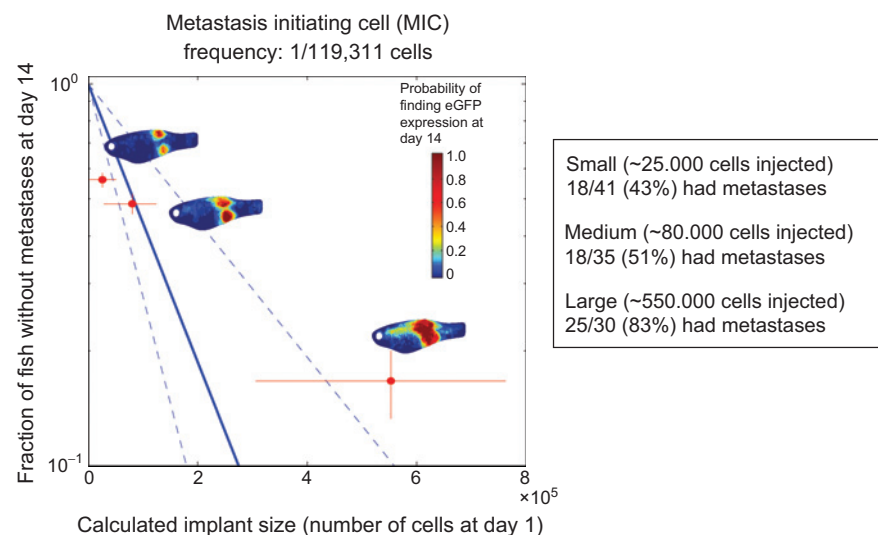
the fish received, we used this to calculate MIC. We estimate 1 MIC per 119,311 cells (lower bound = 1/78,019; upper bound = 1/228,233), meaning that this is the frequency of cells within the ZMEL1 population capable of giving rise to measurable distant metastases within 14 days. This is in agreement with other reports indicating that the frequency of cells capable of completing all steps in the metastatic cascade is quite rare (40, 41). These two measures, the μ score and the MIC frequency, are key measures of metastasis in the zebrafish. Having such quantitative measures is essential to detecting changes in metastatic efficiency during experimental perturbations to either the cells or the recipient host background.

Pigmentation and metastatic progression

Finally, we wished to understand the characteristics of these rare cells capable of metastasis. We noted a significant discrepancy between the appearance of pigmentation and GFP in the recipient animals (Fig. 6A), suggesting that pigment status and metastatic progression were related. In the representative fish shown in Fig. 6A, at 2 weeks after transplant, brightfield imaging (Fig. 6A, left) showed a deeply pigmented, black mass at the implant site, with sharp borders and no obvious metastatic lesions. In contrast, examination of the same fish under GFP (Fig. 6A, right) showed that the implanted mass has several protrusions in the dorsal direction, along with multiple anterior metastases. This suggested that the cells that leave the implant site are likely unpigmented and less differentiated melanocytes. To quantify this, we created composite heatmap images depicting the average level of black pigmentation within the GFP-positive regions at days 7 and 14 (Fig. 6B). This demonstrated that the primary implant site (the center of which is denoted by the red dot) was far more pigmented than the distant anterior metastases. We then determined the distance from the implant site versus the degree of pigmentation (Fig. 6C). This demonstrates a clear inverse relationship: the cells

furthest away from the implant site are nearly all unpigmented, whereas those at the implant site are strongly pigmented.

Although the tumor from which ZMEL1 was originally derived was highly pigmented, the ZMEL1 line in culture shows no evidence of pigmentation, suggesting the cells only become pigmented in vivo. To confirm this, we examined the behavior of the transplanted ZMEL1 cells using time lapse imaging, in which we took one picture per day over a range of 21 to 30 days. As shown in Supplementary Video S2, the implant site becomes large and pigmented prior to the metastases, which are initially only GFP positive before becoming pigmented as well. Over time, once the metastases are completely engrafted, usually even those cells too become pigmented. To determine if this effect was specific to the ZMEL1 line, we also performed transplantation of several BRAF^{V600E};p53$^{-/-}$ primary transgenic melanomas (Supplementary Fig. S1) and found that both the primary engraftment site and metastases become pigmented as well, indicating that melanoma cells retain significant differentiation plasticity: they are unpigmented in vitro, become pigmented when implanted into the primary site in the fish, are unpigmented while metastasizing, and then again become pigmented in the new site of dissemination. These observations are consistent with data from mammalian systems showing that metastatic cells are initially less differentiated (42).

Discussion

We have described a zebrafish system for studying melanoma metastasis, which has all of the components necessary to study both cell intrinsic and microenvironmental regulators of this process at large scale. The isolation of fluorescent zebrafish cell lines, which closely resemble the human disease and which can be easily genetically modified using overexpression or CRISPR cassettes, opens up the possibility to perform genome-wide screens to find modifiers of metastasis. The capacity for in vivo imaging using the transparent casper recipient, which allows for

A

B Average pigmentation level within eGFP positive areas (difference in grayscale intensity compared to D1)

Day 7

Day 14

1 mm • Approximate location of injection site

C

Average pigmentation level within GFP positive areas (AU)

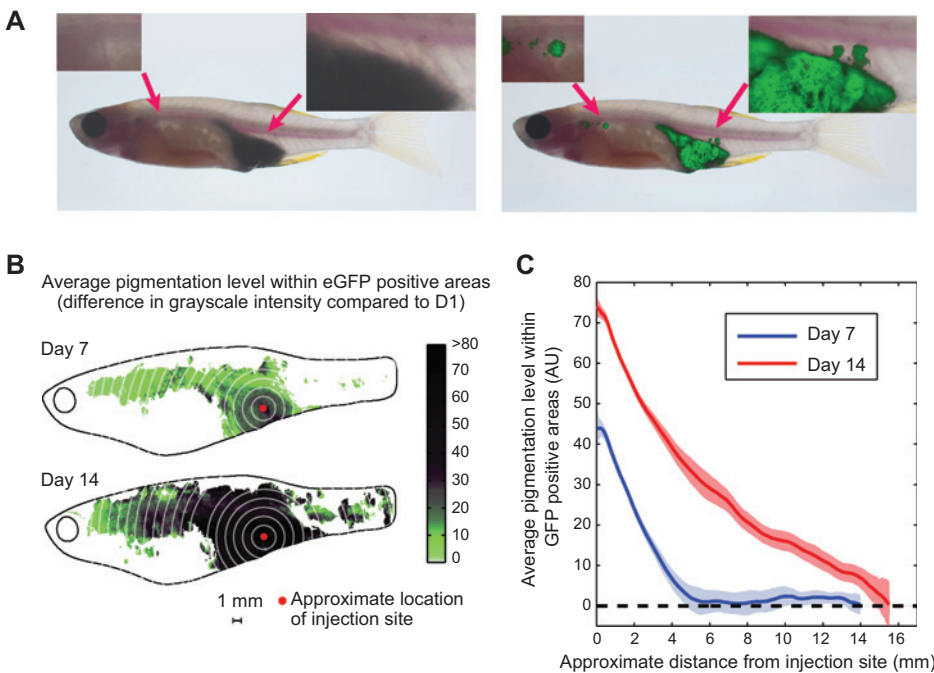Approximate distance from injection site (mm)

— Day 7
— Day 14

Figure 6.
Pigmentation status as related to metastatic capacity. A, representative fish is shown under brightfield (left) and GFP (right) imaging. This reveals a significant discrepancy between pigmented, melanized cells, and metastases. The tumor under brightfield appears smooth bordered and deeply pigmented, with no metastatic lesions. In contrast, GFP imaging of the same fish shows that the local tumor has irregular protrusions dorsally and several anterior metastases. B, composite heatmap of a group of 53 fish showing the relationship between pigmentation and metastasis at days 7 and 14 after transplant, suggesting that the further the cells are from the implant site (red dot), the more likely they are to be unpigmented. C, quantification of the heatmap image shown in B, measuring both distance from injection site along with pigmentation level. This demonstrates a clear inverse relationship, such that the cells capable of furthest travel are largely unpigmented.

visualization at the single-cell level, enables a finer resolution view of micro to macrometastatic progression than is currently achievable in murine models. A particular strength of such high-resolution imaging may be the study of tumor cell extravasation at distant sites, one of the most difficult parts of the metastatic cascade to analyze using current murine models.

We find that the embryonic microenvironment augments metastatic growth compared with the adult, strongly suggesting that the microenvironment is a dominant force in establishing successful metastatic spread. Because it is now straightforward to make CRISPR zebrafish recipient fish carrying germline or somatic mutations of nearly any microenvironmental gene, we envision that a major use of our model will be in screens in which ZMEL1 cells are transplanted into these modified recipient fish. This will allow for a direct assessment of which genes in the microenvironment act as modifiers of disseminated tumor growth at a scale not achievable in other vertebrate systems.

Each of the assays described here has distinct strengths and caveats. The adult *casper* assay is robust and recapitulates the microenvironment present when most melanomas in humans form, i.e., during the postembryonic period. However, because the animals must be immunocompromised to prevent rejection of the ZMEL1 cells, its capacity for studying immune regulation of metastasis is limited. The embryo assay has the distinct advantage of a largely intact immune system, and because the 2-day-old animal is much smaller than the adults at 4 to 6 months described above (where we used 100,000–1,000,000 cells), we need only transplant between 50 and 150 ZMEL1 cells into each 2-day-old recipient. These advantages are partially offset by the obvious growth-promoting effects of the embryonic microenvironment, which likely accounts for the rapidity of disease progression. It is likely that different investigators will find advantages to either of these assays, depending upon the particular question being addressed.

One of the major strengths of studying metastasis in the zebrafish is related to the achievable scale of the experiments. Each individual fish at 6 weeks of age measures approximately $0.021 cm^3$, in contrast with an average mouse at that age that measures approximately $73 cm^3$. On a size basis, for every 1 mouse, it is possible to study approximately 3,000 young zebrafish. Even in a modest-sized zebrafish facility, this opens up a wide range of studies probing metastatic biology that would not be possible in traditional murine systems. Because of the intrinsic heterogeneity of the metastatic state, the zebrafish offers considerable statistical power to discern even moderate modifiers of the metastatic phenotype.

It is likely that some aspects of metastatic biology in a zebrafish will be mechanistically distinct from that in human patients, a caveat for all model systems. In some cases, findings in fish have not translated well to humans (43), yet in others we have seen remarkable conservation of core pathways and genes. For example, findings in zebrafish have resulted in at least two clinical trials in human cancer patients (6, 44, 45), including one specifically focused on melanoma. Because the number of labs currently using zebrafish to study metastasis is limited, it will require a great deal of study before we can begin to understand the similarities, and differences, between fish and human metastasis. The tools described here are an integral component of opening up this line of studies. We anticipate that these methods will be readily extended outside of melanoma into other tumor types, making it broadly applicable to cancer investigators with diverse interests.

Disclosure of Potential Conflicts of Interest

L. Zon has ownership interest (including patents) in and is a consultant/advisory board member for Fate Therapeutics and Scholar Rock. No potential conflicts of interest were disclosed by the other authors.

Authors' Contributions

Conception and design: K. Ratnakumar, A.J. McMahon, L.I. Zon, J.B. Xavier, R.M. White
Development of methodology: S. Heilmann, K. Ratnakumar, E.M. Langdon, I.S. Kim, N.R. Campbell, E.B. Perry, A.J. McMahon, E. van Rooijen, R.O. Hynes, J.B. Xavier, R.M. White
Acquisition of data (provided animals, acquired and managed patients, provided facilities, etc.): K. Ratnakumar, E.M. Langdon, I.S. Kim, N.R. Campbell, C.K. Kaufman, R.M. White
Analysis and interpretation of data (e.g., statistical analysis, biostatistics, computational analysis): S. Heilmann, E.M. Langdon, I.S. Kim, N.R. Campbell, W. Lee, C.A. Iacobuzio-Donahue, J.B. Xavier, R.M. White
Writing, review, and/or revision of the manuscript: S. Heilmann, K. Ratnakumar, N.R. Campbell, E.B. Perry, A.J. McMahon, W. Lee, R.O. Hynes, J.B. Xavier, R.M. White
Administrative, technical, or material support (i.e., reporting or organizing data, constructing databases): S. Heilmann, E.R. Kansler, I.S. Kim, R.M. White
Study supervision: K. Ratnakumar, R.O. Hynes, J.B. Xavier, R.M. White

References

1. Bos PD, Nguyen DX, Massague J. Modeling metastasis in the mouse. Curr Opin Pharmacol 2010;10:571–7.
2. Quail DF, Joyce JA. Microenvironmental regulation of tumor progression and metastasis. Nat Med 2013;19:1423–37.
3. Labelle M, Begum S, Hynes RO. Direct signaling between platelets and cancer cells induces an epithelial-mesenchymal-like transition and promotes metastasis. Cancer Cell 2011;20:576–90.
4. White R, Rose K, Zon L. Zebrafish cancer: the state of the art and the path forward. Nat Rev Cancer 2013;13:624–36.
5. Patton EE, Widlund HR, Kutok JL, Kopani KR, Amatruda JF, Murphey RD, et al. BRAF mutations are sufficient to promote nevi formation and cooperate with p53 in the genesis of melanoma. Curr Biol 2005;15:249–54.
6. White RM, Cech J, Ratanasirintrawoot S, Lin CY, Rahl PB, Burke CJ, et al. DHODH modulates transcriptional elongation in the neural crest and melanoma. Nature 2011;471:518–22.
7. Ceol CJ, Houvras Y, Jane-Valbuena J, Bilodeau S, Orlando DA, Battisti V, et al. The histone methyltransferase SETDB1 is recurrently

amplified in melanoma and accelerates its onset. Nature 2011;471: 513–7.

8. White RM, Sessa A, Burke C, Bowman T, LeBlanc J, Ceol C, et al. Transparent adult zebrafish as a tool for in vivo transplantation analysis. Cell Stem Cell 2008;2:183–9.

9. Zhang L, Alt C, Li P, White RM, Zon LI, Wei X, et al. An optical platform for cell tracking in adult zebrafish. Cytometry A 2012;81:176–82.

10. Hruscha A, Krawitz P, Rechenberg A, Heinrich V, Hecht J, Haass C, et al. Efficient CRISPR/Cas9 genome editing with low off-target effects in zebrafish. Development 2013;140:4982–7.

11. Sung YH, Kim JM, Kim HT, Lee J, Jeon J, Jin Y, et al. Highly efficient gene knockout in mice and zebrafish with RNA-guided endonucleases. Genome Res 2014;24:125–31.

12. UCSC Genome Browser. Available from: http://genome.ucsc.edu/.

13. EMBL EBI. Available from: http://www.ebi.ac.uk/ena.

14. Heilmann S. Matlab-fish-image-analysis. [Online repository]. 2015; Available from: https://github.com/SnowballTheThird/Matlab-fish-image-analysis.

15. Yen J, White RM, Wedge DC, Van Loo P, de Ridder J, Capper A, et al. The genetic heterogeneity and mutational burden of engineered melanomas in zebrafish models. Genome Biol 2013;14:R113.

16. Minn AJ, Gupta GP, Siegel PM, Bos PD, Shu W, Giri DD, et al. Genes that mediate breast cancer metastasis to lung. Nature 2005;436:518–24.

17. Bos PD, Zhang XH, Nadal C, Shu W, Gomis RR, Nguyen DX, et al. Genes that mediate breast cancer metastasis to the brain. Nature 2009;459:1005–9.

18. Soo JK, Ross AD, Bennett DC. Isolation and culture of melanoma and naevus cells and cell lines. Methods Mol Biol 2011;731:141–50.

19. Fogh J, Fogh JM, Orfeo T. One hundred and twenty-seven cultured human tumor cell lines producing tumors in nude mice. J Natl Cancer Inst 1977;59:221–6.

20. Subramanian A, Tamayo P, Mootha VK, Mukherjee S, Ebert BL, Gillette MA, et al. Gene set enrichment analysis: a knowledge-based approach for interpreting genome-wide expression profiles. Proc Natl Acad Sci U S A 2005;102:15545–50.

21. Lee JK, Havaleshko DM, Cho H, Weinstein JN, Kaldjian EP, Karpovich J, et al. A strategy for predicting the chemosensitivity of human cancers and its application to drug discovery. Proc Natl Acad Sci U S A 2007;104:13086–91.

22. Graf SA, Busch C, Bosserhoff AK, Besch R, Berking C. SOX10 Promotes Melanoma Cell Invasion by Regulating Melanoma Inhibitory Activity. J Invest Dermatol 2014;134:2212–20.

23. Cronin JC, Watkins-Chow DE, Incao A, Hasskamp JH, Schonewolf N, Aoude LG, et al. SOX10 ablation arrests cell cycle, induces senescence, and suppresses melanomagenesis. Cancer Res 2013;73:5709–18.

24. Ronnstrand L, Phung B. Enhanced SOX10 and KIT expression in cutaneous melanoma. Med Oncol 2013;30:648.

25. Garraway LA, Widlund HR, Rubin MA, Getz G, Berger AJ, Ramaswamy S, et al. Integrative genomic analyses identify MITF as a lineage survival oncogene amplified in malignant melanoma. Nature 2005;436:117–22.

26. Yokoyama S, Woods SL, Boyle GM, Aoude LG, MacGregor S, Zismann V, et al. A novel recurrent mutation in MITF predisposes to familial and sporadic melanoma. Nature 2011;480:99–103.

27. Cruz-Munoz W, Jaramillo ML, Man S, Xu P, Banville M, Collins C, et al. Roles for endothelin receptor B and BCL2A1 in spontaneous CNS metastasis of melanoma. Cancer Res 2012;72:4909–19.

28. Lahav R, Suva ML, Rimoldi D, Patterson PH, Stamenkovic I. Endothelin receptor B inhibition triggers apoptosis and enhances angiogenesis in melanomas. Cancer Res 2004;64:8945–53.

29. Bollag G, Tsai J, Zhang J, Zhang C, Ibrahim P, Nolop K, et al. Vemurafenib: the first drug approved for BRAF-mutant cancer. Nat Rev Drug Discov 2012;11:873–86.

30. Huang MH, Lee JH, Chang YJ, Tsai HH, Lin YL, Lin AM, et al. MEK inhibitors reverse resistance in epidermal growth factor receptor mutation lung cancer cells with acquired resistance to gefitinib. Mol Oncol 2013;7:112–20.

31. Das Thakur M, Salangsang F, Landman AS, Sellers WR, Pryer NK, Levesque MP, et al. Modelling vemurafenib resistance in melanoma reveals a strategy to forestall drug resistance. Nature 2013;494:251–5.

32. Nazarian R, Shi H, Wang Q, Kong X, Koya RC, Lee H, et al. Melanomas acquire resistance to B-RAF(V600E) inhibition by RTK or N-RAS upregulation. Nature 2010;468:973–7.

33. Ma D, Zhang J, Lin HF, Italiano J, Handin RI. The identification and characterization of zebrafish hematopoietic stem cells. Blood 2011;118: 289–97.

34. Luo R, An M, Arduini BL, Henion PD. Specific pan-neural crest expression of zebrafish Crestin throughout embryonic development. Dev Dyn 2001;220:169–74.

35. Leong SP, Tseng WW. Micrometastatic cancer cells in lymph nodes, bone marrow, and blood: Clinical significance and biologic implications. CA Cancer J Clin 2014;64:195–206.

36. Kaliks RA, Silveira PA, Osawa A, Campregher PV, Bacal NS, Velloso ED. Metastatic melanoma mimicking acute leukaemia. Br J Haematol 2014; 165:1.

37. Serrier C, Lesesve JF. Metastatic malignant melanoma in the bone marrow. Blood 2013;121:721.

38. Hu Y, Smyth GK. ELDA: extreme limiting dilution analysis for comparing depleted and enriched populations in stem cell and other assays. J Immunol Methods 2009;347:70–8.

39. Blackburn JS, Liu S, Langenau DM. Quantifying the frequency of tumor-propagating cells using limiting dilution cell transplantation in syngeneic zebrafish. J Vis Exp 2011:e2790.

40. Singh M, Manoranjan B, Mahendram S, McFarlane N, Venugopal C, Singh SK. Brain metastasis-initiating cells: survival of the fittest. Int J Mol Sci 2014;15:9117–33.

41. Valiente M, Obenauf AC, Jin X, Chen Q, Zhang XH, Lee DJ, et al. Serpins promote cancer cell survival and vascular co-option in brain metastasis. Cell 2014;156:1002–16.

42. Pinner S, Jordan P, Sharrock K, Bazley L, Collinson L, Marais R, et al. Intravital imaging reveals transient changes in pigment production and Brn2 expression during metastatic melanoma dissemination. Cancer Res 2009;69:7969–77.

43. Stern HM, Murphey RD, Shepard JL, Amatruda JF, Straub CT, Pfaff KL, et al. Small molecules that delay S phase suppress a zebrafish bmyb mutant. Nat Chem Biol 2005;1:366–70.

44. Goessling W, Allen RS, Guan X, Jin P, Uchida N, Dovey M, et al. Prostaglandin E2 enhances human cord blood stem cell xenotransplants and shows long-term safety in preclinical nonhuman primate transplant models. Cell Stem Cell 2011;8:445–58.

45. North TE, Goessling W, Walkley CR, Lengerke C, Kopani KR, Lord AM, et al. Prostaglandin E2 regulates vertebrate haematopoietic stem cell homeostasis. Nature 2007;447:1007–11.